Ocean Engineering 173 (2019) 851–866

Contents lists available at ScienceDirect

Ocean Engineering

journal homepage: www.elsevier.com/locate/oceaneng

Design conditions for waves and water levels using extreme value analysis with covariates

Graham Feld[a], David Randell[b], Emma Ross[b], Philip Jonathan[c,d,*]

[a] Shell UK, Aberdeen, AB12 3FY, United Kingdom
[b] Shell Global Solutions International BV, Amsterdam, the Netherlands
[c] Shell Research Limited, London, SE1 7NA, United Kingdom
[d] Department of Mathematics and Statistics, Lancaster University, LA1 4YW, United Kingdom

ARTICLE INFO

Keywords:
Metocean design
Extreme
Total extreme water level
Non-stationary
Uncertainty

ABSTRACT

This article presents a step-by-step procedure for estimation of the joint distribution of N-year maximum significant wave height, individual wave and crest heights, and total water level, accommodating the effects of directional and seasonal variation, surge and tide. The approach is based on non-stationary extreme value analysis of peaks over threshold incorporating careful uncertainty quantification, and is illustrated for a North Sea location using hindcast data. The article further provides a brief overview of the development of a regulatory framework for specification of design conditions for total water level over the past half century.

1. Introduction

Extremes of wave height and total water level (TWL) are key parameters for the design of fixed platforms in the offshore environment. Previous papers (e.g. Feld et al. (2015), Randell et al. (2015)) have described an approach to non-stationary extreme value analysis (henceforth called "CEVA", abbreviating "Covariate Extreme Value Analysis") for estimating N-year maxima of significant wave height, individual wave and crest heights, taking into account the variation in seasonal and directional covariates. Waves that impact the topsides and supporting beams of offshore structures are particularly significant since they result in a rapid increase in loading with inundation level. Extremes of TWL, namely the combination of wave crest and still water level (SWL, itself the sum of tide and storm surge), can cause bigger loads still, and are often of greater importance to the structural engineer than crest height alone. This paper builds on the approach described in previous papers to also include SWL effects in a manner which is consistent with the wave modelling methodology and which preserves the relationships between waves, storm surge and tidal levels that are observed within storms.

The underlying approach to the estimation of the wave component of TWL is based upon modelling storm peak events on a directional-seasonal covariate domain, described in outline in Section 4. Whilst this approach captures the storm peaks appropriately, in order to determine the maximum TWL within each storm, it is necessary to model more than just the peak sea state. This is due to both the random nature of large individual wave crests within sea states near to the peak and also to the characteristics of the inter-relationships between waves, tide and surge. Both of these effects may result in the highest water level during a storm occurring at a time of lower significant wave height (H_S) but higher tide and/or surge.

In order to represent the total water level variability throughout a storm event, therefore, representative *storm trajectories* are derived which aim to capture the variability of all of the key wave (Section 5) and surge (Section 6) parameters as the storm develops both temporally and directionally. These trajectories can then be appropriately re-scaled in order to match the severity of storm peaks randomly selected from the fitted extremal model.

To estimate maximum TWL in a storm, all these modelling components, i.e. storm peak modelling, wave and surge storm trajectory selection and tidal variations, need to be brought together and combined with the short-term variability of individual crest heights. In this way, for each simulated sea state in each storm event, individual maximum crests are randomly sampled and added to appropriately selected surge and tidal level. This process, explained in Section 7, is then repeated for all randomly-simulated storms over the return period of interest. For each period of simulation the maximum TWL for each direction and day-of-year are retained. This allows extreme values of TWL for any directional-seasonal combination to be subsequently extracted and these can then further be aggregated to derive all-year and omnidirectional extremes in a statistically consistent manner. This final simulation is described in Section 8.

* Corresponding author. Shell Research Limited, London, SE1 7NA, United Kingdom.
E-mail address: philip.jonathan@shell.com (P. Jonathan).

https://doi.org/10.1016/j.oceaneng.2018.10.027
Received 3 May 2018; Received in revised form 7 September 2018; Accepted 21 October 2018

This modelling procedure allows all extremes that may be required for design and operational purposes to be derived in a single analysis. For example, seasonal criteria for installation activities are readily available; or, a re-alignment of a structure during the design phase can be easily accommodated by simply aggregating across different sets of directional sectors.

Throughout this whole process, uncertainties are propagated into the estimated distribution of the *N*-year maximum TWL, using the methods described. These uncertainties are captured by using bootstrapping of the original storm peak data, a range of wave and surge storm trajectory shapes, different tidal phases, a range of extreme value thresholds, random sampling of H_S, and random sampling of individual crest heights.

2. Background

For the offshore environment, we assume that TWL is defined as the sum of individual crest, surge and tidal components. The importance of TWL has been explored particularly within two areas of study (a) coastal flooding and over-topping, and (b) wave impact on marine bottom-founded structures. In the first of these, annual maxima from long time series were traditionally used as the basis for extrapolating to long return periods but based on SWL, i.e. combined tide and surge. This approach means, however, that many significant surge events will be excluded if they happen to occur at low tide and it also does not make the best use of the available data since only a single event per year is included. The combined effects of decoupled tide and surge were modelled in Pugh and Vassie (1978) by the Joint Probability Method (JPM) where non-parametric probability distributions for both were derived and, assuming independence, recombined statistically to obtain the statistics of overall SWL. In order to extrapolate to longer return periods an empirically-selected log distribution was fitted to the tail of positive surges. The approach made better use of the data by using all hourly samples but in so doing introduced a data set which consisted of dependent samples. This introduced a bias into the estimate of the non-exceedance probability associated with given return periods.

Despite the shortcomings of the method it has been widely applied although the method was subsequently revised by Tawn (1992) to decluster the surge data into independent events, to smooth the observed magnitudes and to fit a more statistically-justified generalised Pareto distribution (GPD) to the tail of the surge distribution. An empirical approach for adjusting the surge distribution for different tidal levels was also presented for application to those shallow locations where this was relevant. Hawkes et al. (2002) proposed a joint model for water level, wave height, wave steepness and their dependence. An extension of the JPM for application to cases with more than two variables was described by Liu et al. (2010) in the “Direct JPM” in which a multi-dimensional histogram was set up to include wave run up in addition to tide and surge. In this approach the characteristics of dependence between the three were explicitly captured by using an empirical non-parametric method although the details used for extrapolation beyond the length of the data set are unclear. Shevchenko and Ivelskaya (2015) broadened and generalised the original JPM to include a description of seasonal variability in mean sea level within the tidal harmonics and used the Gumbel distribution to extrapolate both surge and tsunami levels to longer return periods. However, any joint probability characteristics between the parameters were not explicitly modelled in this approach.

More sophisticated modelling approaches to joint probability in general have been developed by Heffernan and Tawn (2004) which describe the relationship of variable *Y* conditional on the value of another extreme variable *X* following transformation to a standard (typically Laplace) marginal scale

$$Y|\{X = x\} \quad = \quad ax + x^b W \tag{1}$$

where $a \in [-1,1]$ and $b \in (-\infty, 1]$ are fitted parameters and *W* represents a residual process with unknown distribution, assumed Gaussian for fitting only. Typically a generalised Pareto distribution (GPD) is used to fit each marginal distribution of peaks over threshold. The approach can be extended to any number of variables in which each is conditional upon the value of a single conditioning variable that exceeds a certain extremal threshold. Gouldby et al. (2014) applied this approach to the study of coastal over-topping and overflow which included SWL and wave components. Once the model was fitted, a Monte Carlo approach was used in which a single parameter was sampled randomly and the relationship presented above was used (including sampling from the distribution of residuals, *W*) to determine associated values of other parameters in order to model for long return periods.

In terms of setting the deck height of offshore structures and the determination of extreme TWL in the North Sea, the design recipe in the 1970s and early 80s was based on a 1.5 m clearance over and above a combination of the 50-year crest height, the 50-year surge and the mean high water spring (MHWS) tide (UK HMSO, 1974). During the 1980s, the key return period was increased to 100 years and some simple allowance was given for joint probabilities between tide and surge on the assumption of two Gaussian parameters between which a correlation coefficient could be defined (UK Department of Energy, 1990).

By 1998, the UK Health and Safety Executive dictated that a structure needed to withstand the 10,000-year TWL with no additional air gap but no clear guidance was given as to how the TWL should be derived. At this time, therefore, certain approximate methods were developed within the industry based on empirically-derived relationships founded on considerations such as storm length versus length of tidal cycle and rules of thumb relating crest heights from one return period to another. One such method for the 10,000-year TWL, TWL_{10000}, which was adopted by Shell and BP in 2000 was the so-called “Interim method”

$$\mathrm{TWL}_{10000} = C_{1000} + \frac{3}{4}(\mathrm{MHW} - \mathrm{MSL}) + S_1^+ \tag{2}$$

where MHW is the mean tidal high water, S_1^+ is the 1-year positive surge, C_{1000} is the 1000-year crest height, and MSL is mean sea level. A second approach was described in Leggett et al. (2007) for the central (CNS) and southern (SNS) North Sea

$$\begin{aligned} &\text{CNS: } \mathrm{TWL}_{10000} = C_{10000} + \mathrm{MSL} + S_1^+ \\ &\text{SNS: } \mathrm{TWL}_{10000} = C_{10000} + \mathrm{MSL} + S_3^+ \end{aligned} \tag{3}$$

where S_3^+ is the 3-year positive surge, and where subscript 10000 refers to the 10,000-year value of the corresponding quantities; however this approach - based on consideration of only selected combinations of crest height, tide and surge rather than a general investigation of the worst possible combinations - was not generically applicable.

ISO19902 (2007) presented a range of TWL values for an offshore location utilizing relationships between tide, surge and crest and this was based on the approach set out by UK Department of Energy (1990). It provided limiting cases for TWL based on either complete correlation between surge and crest and the completely uncorrelated case. The range provided for TWL was

$$(\sqrt{a^2 + s^2 + t^2},\ \sqrt{(a+s)^2 + t^2}) \tag{4}$$

where *a* is the extreme crest height, *s* is the extreme surge and *t* is the maximum elevation of tide relative to mean sea level.

ISO19901-1 (2005) adopted the Tromans and Vanderschuren (1995) storm-based approach for the determination of individual wave and crest height return values based on the statistical combination of the long-term distribution of storm maxima with the short-term distribution of individual waves. This correctly accounts for the fact that the largest waves in a storm do not necessarily come from the most severe sea state and that the largest waves in a given return period do not necessarily come from the storms with the largest H_S. However,

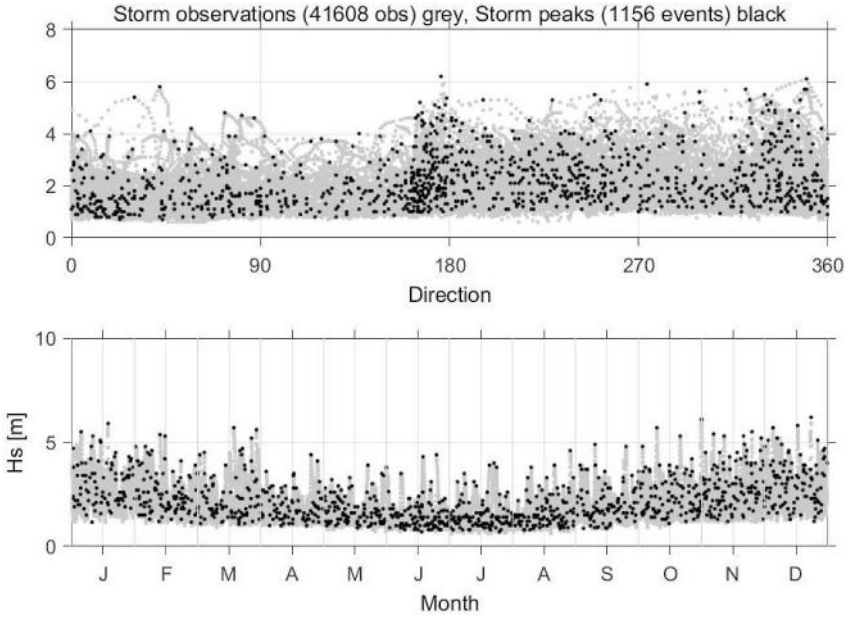

Fig. 1. Example data set: variation of H_S by direction (top) and season (bottom). Grey dots represent all data, black dots represent storm peaks.

there was still no further guidance as to how to combine these crest heights with SWL variations.

In UK Health and Satefy Executive (2009), a Monte Carlo approach was described to combine the approach of Tromans and Vanderschuren (1995) for individual wave crests with a representation of the joint probabilities of waves and surge. Again, though, a simplistic approach was adopted in which once a randomly-selected H_S was selected, the surge of the same percentile was associated with the sea state such that effectively, a perfect correlation was assumed between waves and surge, but a random tide was included. An additional empirical correction factor was then derived from measured data to correct for the degree of correlation.

We note the work of Callaghan et al. (2008), Serafin and Ruggiero (2014), Wahl et al. (2017) and others on simulating wave environments for estimation of erosion and over-topping. Previous papers by some of the current authors have developed the Monte Carlo approach (e.g. Ewans and Jonathan, 2008; Feld et al., 2015) in which the approach of Tromans and Vanderschuren (1995) was adopted for the crests but which allowed for varying characteristics by season and direction in order to better capture the changing statistical populations through the year and by direction.

In order to derive TWL, however, a method for combining these crests with appropriate tides and surges is required, and this is the substance of the current paper.

3. Example data set

For illustrative purposes, a data set from a location in the western half of the Southern North Sea in a water depth of around 20 m has been chosen. The water level data consisted of hourly measurements at an offshore platform between October 2006 and December 2016 and the wave data came from the NORA10 (Norwegian Reanalysis, 10 km wave hindcast model, Reistad et al., 2011) WAM (third generation prognostic wave model, WAMDI, 1988) hindcast grid point closest to the measurement location and covered the same period. A representation of the distribution of H_S by season and direction is shown in Fig. 1 showing the significance of the covariates in determining the severity of any particular directional-seasonal combination. In this plot, all the data points are shown as grey dots and the storm peaks are shown as black dots. Direction is defined as the direction from which storms propagate, measured clockwise from North.

Tides were separated from storm surges by harmonic analysis (using T_Tide software, Pawlowicz et al., 2002) of hourly mean original water level data, with residual level referred to as surge. Fig. 2(a) shows the variability of surge with season with black dots representing all the observed data points; again the seasonality is obvious. A similar plot is shown for tide in Fig. 2(b) where the small equinoctial effect on tides can be seen. The relationship between tide and surge is shown in Fig. 2(c) in which the relationship appears to be random in nature in an overall sense, although there appears to be a slight tendency for the highest surges to have occurred at the extremes of tide either high or low. Fig. 2(d) illustrates the overall relationship between H_S and surge. In this case, the largest surge events are associated with higher H_S values but the scatter indicates that a large H_S does not necessarily imply that a large surge will occur simultaneously.

For definiteness, wave height is defined as the difference between the maximum and minimum values of the ocean surface between consecutive down-crossings of mean water level. Crest height is defined as the maximum value of the ocean surface between an up-crossing and subsequent down-crossing of the mean water level.

4. Storm peak modelling

The details of this approach have been described in previous papers (e.g. Feld et al., 2015). Briefly.

1. A set of directional-seasonal covariate “bins” within which conditions are considered homogeneous is defined. Binning reduces the computational complexity of the covariate description, and hence the complexity of the spline calculations to estimate extreme value (EV) models. Typically, this is based on 32 directional bins (11.25° width) and 24 seasonal bins (approximately 2 weeks long) giving a

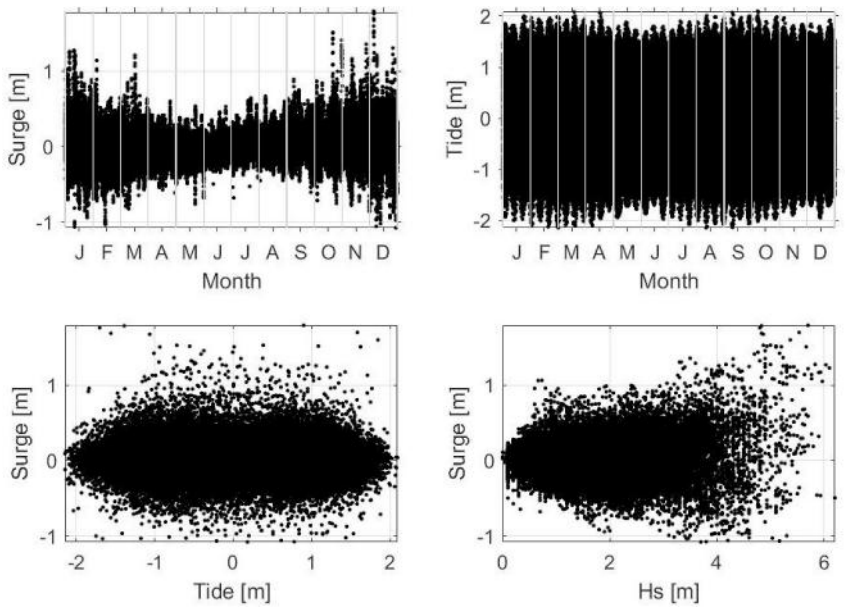

Fig. 2. Example data set: (a) surge on month, (b) tide on month, (c) surge versus tide, both with respect to long-term mean sea level, and (d) surge versus H_S.

total of 768 across the covariate domain.

2. A threshold q for isolation of storm event is defined using a quantile of sea state H_S per directional-seasonal sector. This threshold is typically chosen to correspond to a quantile with constant non-exceedance probability of between approximately 0.5 and 0.75; this produces a sufficient number of storm events whilst keeping the storm length to a manageable size. A quantile is better than a fixed storm threshold since this ensures that calmer seasons and directions are adequately represented in the overall model (and see e.g. Northrop and Jonathan, 2011). The peak of the storm event is captured and characterised by the storm peak H_S (referred to as H_S^{sp} for definiteness where needed), zero-crossing wave period (T_Z), spectral mean period, T_{01}, direction and day of year. Note that T_{01} is defined as $\sqrt{m_0/m_1}$, where m_0 is the zeroth moment and m_1 the first moment of the wave spectrum; T_{01} is a key parameter in the Forristall crest height probability distribution.
3. For each storm, the whole period of exceedance of storm threshold q is also added to the set of historical storm trajectories which can then be associated with synthesized storm peaks (see Section 5).
4. A set of viable EV thresholds ψ for storm peaks is chosen, corresponding to quantiles with non-exceedance probabilities per covariate bin within some reasonable interval. Above ψ, occurrences of storm peaks are assumed to follow a Poisson process (with mean rate ρ), and storm severity described by a generalised Pareto model (with scale parameter σ and shape parameter ξ).
5. The variation of model parameters ψ, ρ, σ and ξ with covariates is described using linear combinations of cubic B-spline functions (or tensor products thereof) defined on the covariate domain. Each spline function has a fixed width but can vary in height. The extent to which spline function height is allowed to vary between adjacent splines is determined by penalty terms and an optimal smoothness chosen using cross-validated penalised maximum likelihood

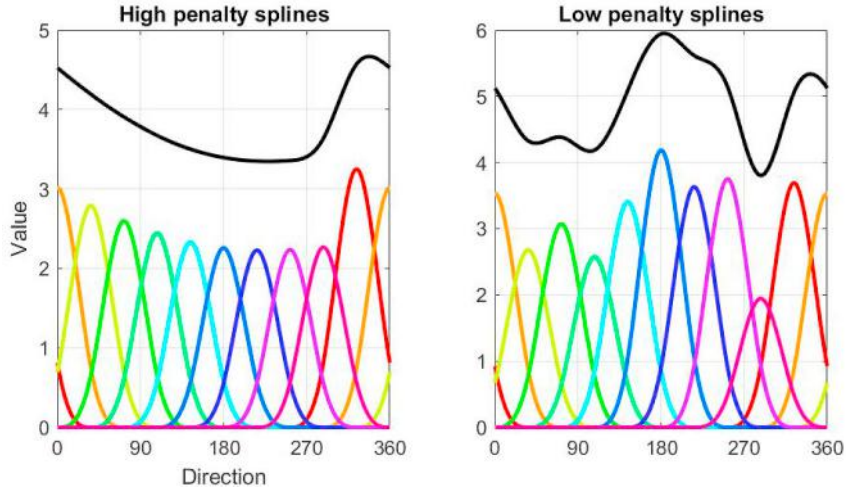

Fig. 3. Illustration of (a) high penalty spline combinations and (b) low penalty splines. The total representation of variability is indicated by the heavy black lines.

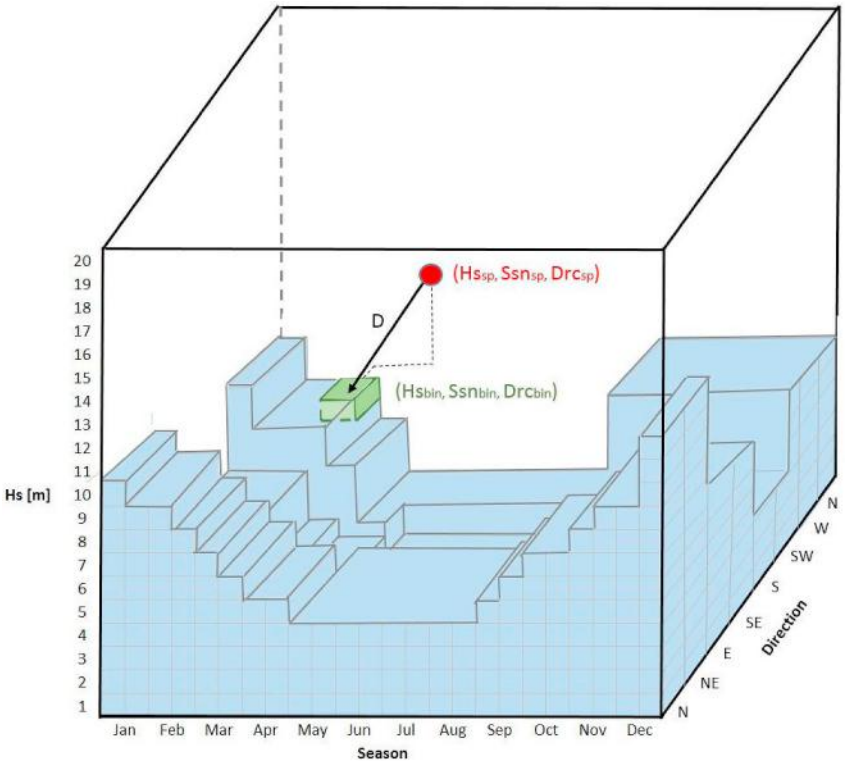

Fig. 4. Representation of distance from a random storm peak at (Hssp, Ssnsp, Drcsp) to each directional-seasonal bin (Hsbin, Ssnbin, Drcbin). The bins which contain storms are indicated by the blue boxes. Each bin contains a population of storm trajectories which are randomly selected. The green bin is closest to the storm peak. (For interpretation of the references to colour in this figure legend, the reader is referred to the Web version of this article.)

estimation. The intention is that spline smoothness is chosen so that the resulting variation in model parameters reflects the underlying natural variability present, whilst preventing over-fitting. A conceptual illustration (unrelated to the current application) of the effect of high and low penalty cases is shown in Fig. 3. In the left-hand case, the variability of heights between adjacent splines is much more constrained than the right-hand case. A penalised likelihood approach is also used to estimate covariate-dependent EV thresholds ψ in 4, above.

6. The procedure for partitioning the covariate domain is explained in (e.g.) Ross et al. (2017). We choose to partition the domain into 32 directional bins of width 11.25°, and 24 seasonal bins of width 15 *seasonal days* (from a year with 360 *seasonal days*). We judge this resolution to be sufficient to capture the main directional and seasonal variation of storm peak significant wave height. The extreme value model therefore uses a total of 768 ($= 32 \times 24$) covariate combinations. For extreme value analysis we assume that neighbouring covariate bins exhibit similar behaviour. This is enforced by *penalising* the local variation of extreme value parameter estimates. We choose the penalty so that the resulting extreme value model has *optimal predictive performance*. In this sense, if there was no predictive evidence in the data related to covariate variation, the extreme value model would be extremely stiff, corresponding effectively to one covariate bin: in this case there would be one bin and 1156 peaks in it for the current application. Further, the *effective number* of covariate degrees of freedom used in the analysis can vary from one (stiff) to 768 (flexible). The actual effective number is chosen to maximise predictive performance using cross-validation. The optimal choice of parameter roughness penality is discussed more fully in Section 6 and illustrated in Fig. 6.

All modelling is performed for 768 covariate combinations. For presentation of results concerning the distribution of N-year maxima, we can combine covariate bins to present exactly the results that the engineer finds most useful. In this work, we present estimates (e.g. Fig. 11 or Fig. 12, discussed in Section 8) on 8 directional octants and 12 seasonal months. However, we can provide estimates of extreme environments using any combinations of covariate bins of interest to the engineer.

Once the storm peak modelling has been completed, a Monte Carlo approach can then be used to simulate a set of random storm peaks for any given return period that reflects the underlying statistical characteristics of the data. To capture uncertainties in this process, the original data can also be bootstrapped and the whole modelling process repeated.

5. Derivation of storm wave trajectory

It is not sufficient to just base the analysis on storm peaks. There are two main reasons for this: (a) an extreme value of TWL in a given directional sector will not necessarily correspond to an occurrence of storm peak H_S in the same directional sector; it may occur as the tail of a storm that peaks in a different directional sector, and (b) when looking at large individual wave and crest values, these may occur during sea states that are not at the peak of storms.

A consequence of this approach is that the largest observed values in each of the directional sectors are not and should not be statistically independent. In practice, however, the data are used in the design process as if they were independent and this means that there is some level of conservatism in the directional extremes. In general, though, the level of dependence is small for bins of size 45° or larger and the biggest effect is on the least severe sectors. If only storm peaks were used to derive extremes, though, the results would be non-conservative so, on balance, the approach described here is preferred. Note that the

effect is not an issue for seasonal sectors since storm lengths are much shorter than the lengths of normal seasonal definitions.

We now assume that trajectories of storms within the database being analysed are representative of the range of storm shapes that may be seen. Clearly, storms of different severities and in different seasons and directions may have different characteristics, so the challenge is to identify storms that have peaks that are *closest* to each randomly-simulated storm peak. To identify these, the observed storm histories are aggregated into a set of bins defined by the storm peak values of H_S, direction and day of year. This is illustrated in Fig. 4 where bins populated with storm peaks from the observed data are indicated in blue.

For every randomly-selected storm peak with characteristics (H_S^{sp}, Drc^{sp}, Ssn^{sp}), indicated by a red dot in the figure, a *distance D* is defined to the centre of every bin (with characteristics ($H_{S_{bin}}^{sp}$, Drc_{bin}^{sp}, Ssn_{bin}^{sp})) for which data is available, namely

$$D^2 = \frac{(H_S^{sp} - H_{S_{bin}}^{sp})^2}{\alpha_{H_S}^2} + \frac{(\mathrm{Ssn}^{sp} - \mathrm{Ssn}_{bin}^{sp})^2}{\alpha_{\mathrm{Ssn}}^2} + \frac{(\mathrm{Drc}^{sp} - \mathrm{Drc}_{bin}^{sp})^2}{\alpha_{\mathrm{Drc}}^2} \quad (5)$$

where superscript *sp* indicates storm peak values, H_S is significant wave height, Ssn is the day of year, Drc is direction and the αs are scaling factors selected for each variable.

The bin that is closest for the selected scaling factors (indicated by the green bin in the figure) is then used as a source of *archetype* storms (and corresponding trajectories) for the storm peak in question. The scaling factors α_{Hs}, α_{Ssn} and α_{Drc} can be adjusted in order to fine-tune the relative importance of the three dimensions for the data set under investigation. The number of archetype storms in each bin can also be adjusted. A large number of storms would produce a more varied array of potential storm shapes, so capturing uncertainty in the storm trajectory, but if the number is set too large then there will be storms that are less similar to the simulated storm peak that are also randomly selected. Suitable values of the α parameters are chosen by inspection of diagnostic plots illustrating the performance of storm trajectory matching using a cross-validation procedure; historical storms are withheld from the analysis in turn, and then used as test cases. We find values of α parameters yielding adequate matching to the storm trajectory for the withheld storms. Typical values of the α parameters are given in Feld et al. (2015).

Once the archetype populations have been established, the trajectories will be randomly selected for association with randomly-simulated storm peaks. If the selected storm trajectory for some archetype (labelled $*$ for definiteness) has peak characteristics H_S^{sp*}, Drc^{sp*} and Ssn^{sp*}, the storm trajectory is then adjusted for association with a storm peak with characteristics H_S^{sp}, Drc^{sp}, Ssn^{sp}, such that (a) all H_S values are scaled by the ratio of H_S^{sp}/H_S^{sp*}, (b) the whole storm history of directions are rotated by $\mathrm{Drc}^{sp} - \mathrm{Drc}^{sp*}$ so that the archetype storm peak direction matches that of the simulated storm peak, and (c) wave periods are scaled such that after scaling, the sea-state steepness $S = 2\pi H_S/(gT_2)$ at every time step does not change.

For further discussion of the storm wave trajectory matching procedure, please see Feld et al. (2015).

6. Still water level modelling

For the determination of TWL, the joint relationship between wave crests, tide and surge needs to be captured. Within the CEVA methodology, the same storm archetype approach that is used for storm wave trajectories is also used to describe the development of surge through storm histories, as outlined in Section 6.1. For locations where the water depth is sufficiently shallow that variations in the water depth can have an effect on the sea states it is important to also capture the tidal variation from that same storm. For deeper-water locations, just the storm surge needs to be available and the tide can be randomly sampled. These tidal approaches are described in Section 6.2.

6.1. Surge modelling

Within the period of each storm, as characterised by the exceedance of H_S above storm threshold q, the storm surge is characterised by its maximum, minimum, median and range, i.e. the difference between the maximum and minimum storm surge as illustrated in Fig. 5.

Linear relationships are then developed between each of these characteristics and the storm peak H_S within each of the directional and seasonal bin combinations giving a total of 768 different fits. The relationship is defined in terms of (a) a selectable quantile of storm peak

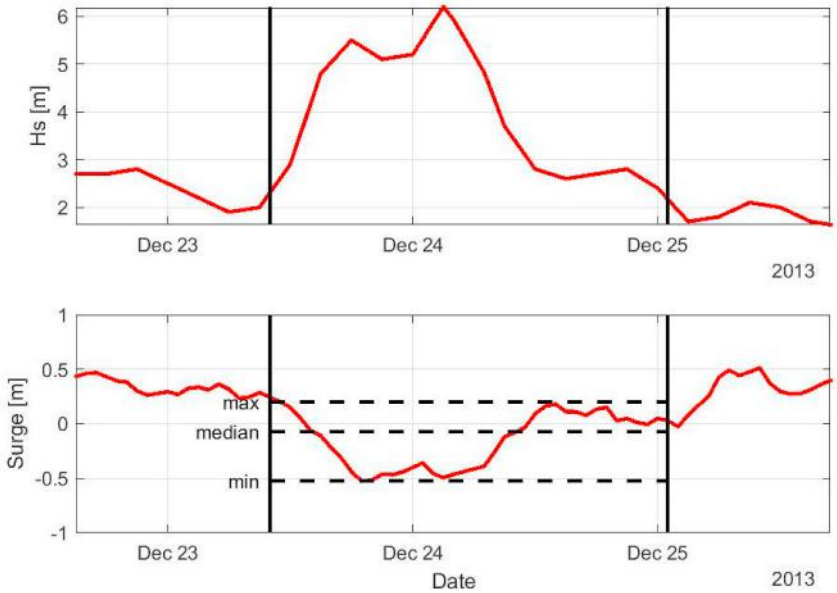

Fig. 5. Storm surge characteristics and definitions. Panel (a) shows H_S in time with vertical black lines representing start and end of storm period. Panel (b) shows the corresponding surge time-series, with minimum, median and maximum values as horizontal dashed black lines.

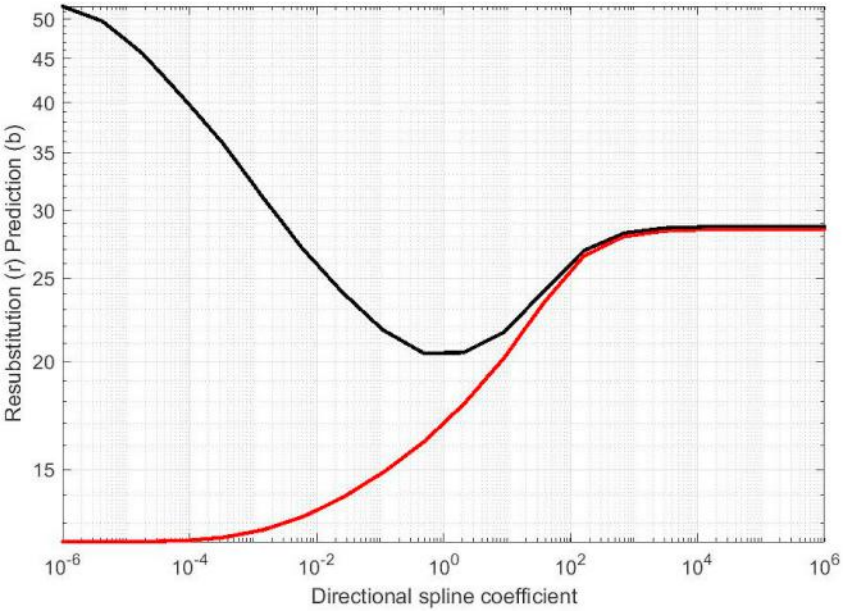

Fig. 6. Selection of optimal spline penalty coefficients for storm surge maximum. Red represents lack of fit, black represents predictive performance. Minimum point of the black line represents the optimum penalty coefficient used for modelling. Similar plots are available for surge minimum, median and range. (For interpretation of the references to colour in this figure legend, the reader is referred to the Web version of this article.)

H_S and the corresponding median value of surge characteristic (together referred to as a *lock point* with value H_S Lock, SurgeLock) and (b) the slope of a linear least-squares fit between the surge characteristic and storm peak H_S (with value Slope). The allowed rate of variability of Slope with direction and season is set using a smoothing B-spline, optimised using cross-validation. For a given covariate bin, the model takes the form

$$\text{Surge} = \text{Slope} \times (H_S - H_S\text{Lock}) + \text{SurgeLock}. \quad (6)$$

Estimation of cross-validation smoothness penalties for Slope (in the case of the surge maxima variable) is illustrated in Fig. 6. The figure shows lack-of-fit from the regression model as a function of Slope smoothness. Red lines illustrate how well the regression model describes variation present in the data as a function of Slope smoothness: as Slope becomes smoother (from left to right) the quality of fit reduces. The black line illustrates how well the regression model is able to *predict* unseen data: at optimum smoothness, the lack-of-predictive-fit is a minimum. This is a classic bias-variance trade-off.

To illustrate for the case of surge maxima, Fig. 7 shows the variability of storm peak H_S lock point, slope and storm surge maximum lock point. Fig. 8 shows 95% uncertainty intervals (UI) for the range of 96 linear fits within each of 8 aggregated directional sectors for the illustrative example for storm surge maximum, surge median and surge minimum characteristics. In these plots, the grey dots represent all the observed combinations of H_S and surge whilst the coloured dots represent the H_S and surge maximum pairs (blue), H_S and surge median pairs (yellow) and H_S and surge minimum pairs (red). Similar plots (not shown) were examined by month. The plots show that in general there is a broadening of surge maximum and surge minimum as H_S increases with surge median in general tending to increase more slowly. This is apparent in plots split both by season and direction. It is also evident that as expected, there are more severe events that occur in the winter months and that the south-east and east are calmer directions.

In order to capture the variability in the relationship between storm surge characteristics and H_S, the residuals of the linear regression relationships, i.e. the differences between observed relationships and the line of best fit are also saved. These are then sampled randomly during the final Monte Carlo analysis and applied to the regression relationship for each storm. Residuals from storm surge characteristics were inspected by direction and season, and did not show obvious structure.

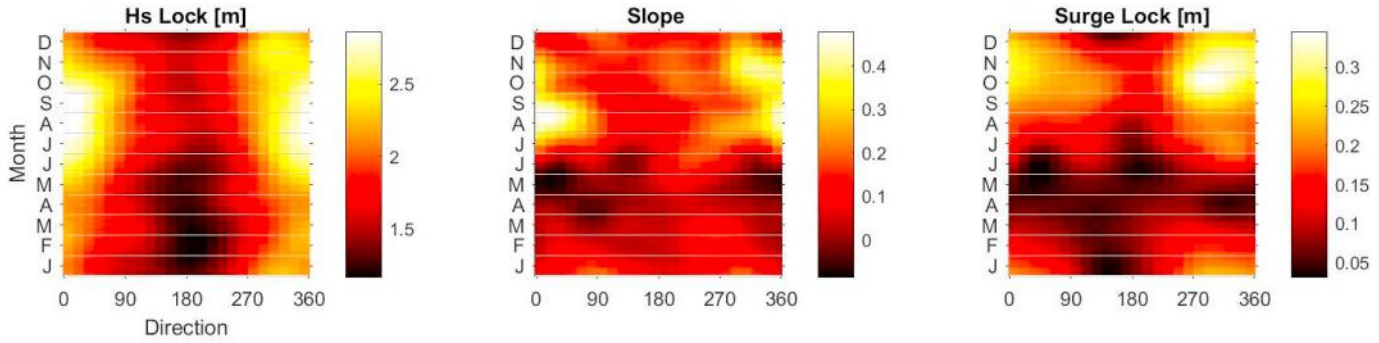

Fig. 7. H_S^{sp} lock (left), slope (middle) and surge lock (right) for storm surge maximum. Similar plots are available for surge minimum, median and range.

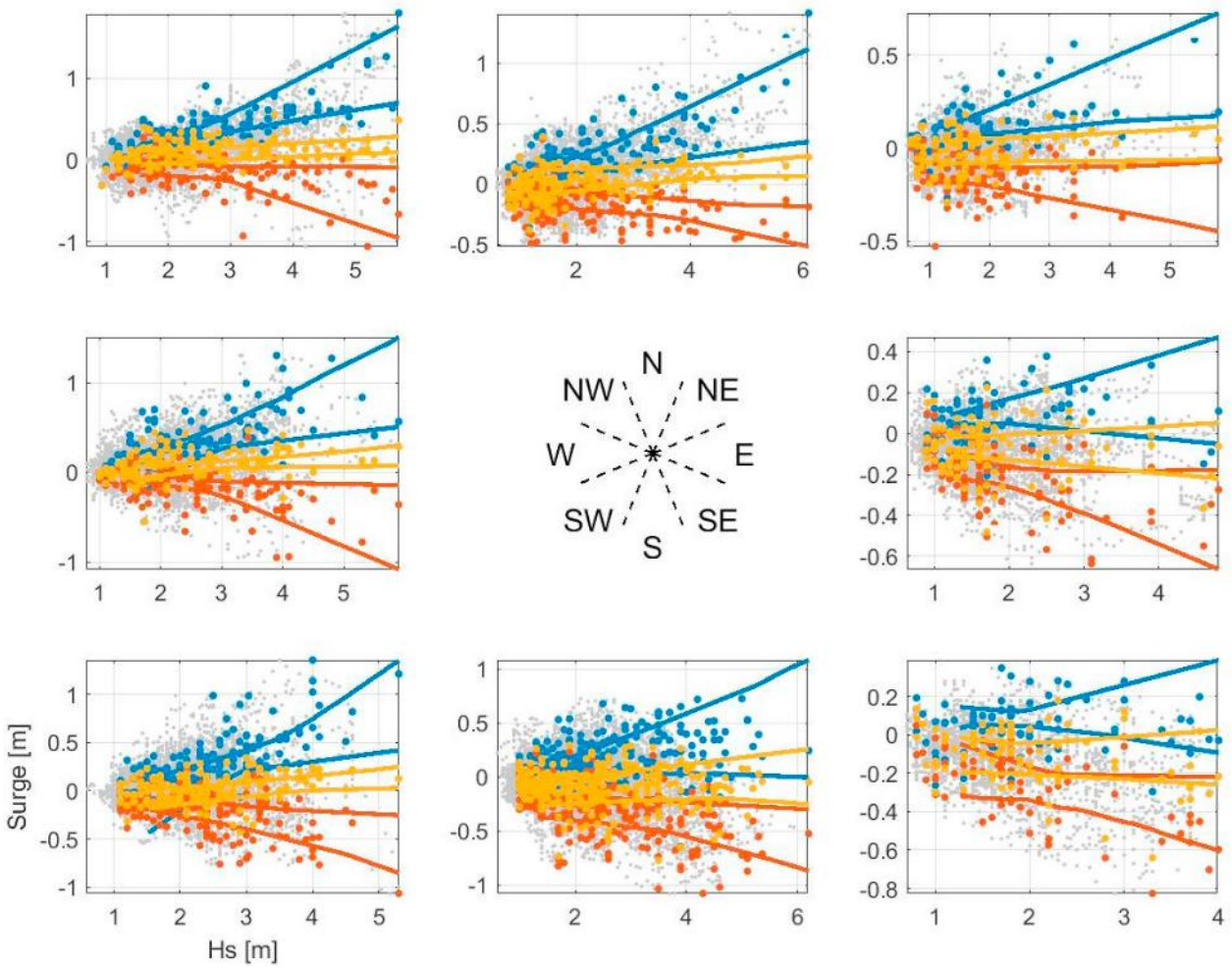

Fig. 8. 95% uncertainty intervals for 96 linear fits within each directional sector of storm surge versus H_S. Surge maximum (blue), median (yellow) and minimum (red). Coloured points show surge maximum, median and minimum values; all other pairs are shown in grey. (For interpretation of the references to colour in this figure legend, the reader is referred to the Web version of this article.)

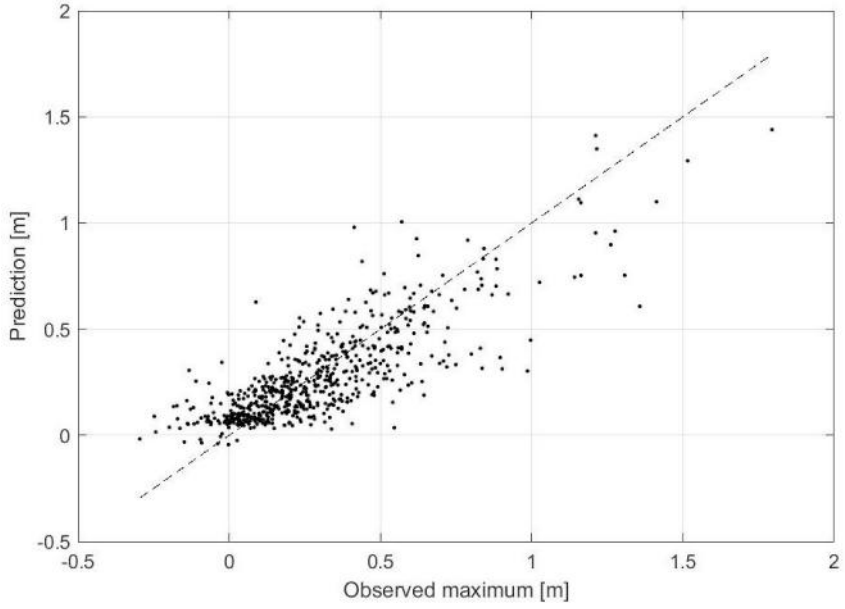

Fig. 9. Observed and predicted storm surge maxima with best-fit line shown. Similar plots are available for storm minima, storm median and storm range.

Residuals are re-sampled during simulation to ensure that the natural variability in relationships is captured rather than collapsing everything onto a single regression relationship. Fig. 9 illustrates the overall performance of the regression model for the storm surge maximum characteristic.

For given simulated storm peak H_S value, we use Equation (6) above to calculate a surge maximum, surge median, surge minimum and surge range for the simulated storm; these values are dependent on the storm peak direction and season of the simulated storm peak event. We refer to these as mxm, mdn, mnm and rng for clarity. We next adjust the matched archetype surge trajectory $\{s_t^*\}$ say (which originally has different values mxm*, mdn*, mnm* and rng* for the surge maximum, median, minimum and range) such that the adjusted archetype surge trajectory $\{s_t\}$ has the desired values corresponding to the simulated storm peak event. There are numerous possible approaches to achieve this. Here we outline a simple linear scaling approach based on matching surge median, surge maximum and surge minimum only. For $s_t^* > \text{mdn}^*$, define s_t such that

$$\frac{s_t - \text{mdn}}{\text{mxm} - \text{mdn}} = \frac{s_t^* - \text{mdn}^*}{\text{mxm}^* - \text{mdn}^*} \tag{7}$$

and when $s_t^* \leq \text{mdn}^*$, define s_t such that

$$\frac{\text{mdn} - s_t}{\text{mdn} - \text{mnm}} = \frac{\text{mdn}^* - s_t^*}{\text{mdn}^* - \text{mnm}^*} \quad . \tag{8}$$

6.2. Tidal modelling

When a random storm is simulated the waves and surge are sampled from the same archetype storm, so retaining the relationship between these components. For shallower-water locations, the tidal component itself is sampled from the same storm as the waves and surge, but the tidal component is not re-scaled. In most hindcasts that are available, the effect of the variation in still water level on H_S is not captured as they are run with a constant water depth. For this reason, it is often better to use measured wave and water level records to establish the relationships between H_S and still water levels. An example of the impact of water level on the H_S time trace is shown in Fig. 10.

7. Simulation of TWL and related variables

To obtain a single realisation of maximum TWL (and its components) for a single storm, the following procedure is used. We start by (a) simulating a storm peak direction and season (from the Poisson rate model), and a storm peak H_S (from the extreme value model). Then (b) we select a historical archetype storm trajectory (of sea-state H_S with direction and season in time, and surge in time) with similar storm peak characteristics to the simulated storm peak (as described in Section 5), and (c) rescale the storm trajectory (sea-state H_S) characteristics (as described in Section 5) so that they agree with the simulated storm peak. Then (d) we rescale the surge trajectory (as described in Section 6). Next (e), we sample a random historical interval of tide to associate with the storm. Then (f) we estimate the water depth for every sea state using the SWL components of tide and surge, and the mean sea level above bed. Subsequently (g) we randomly sample maximum individual crest heights for each sea state using probability distributions based on the corresponding water depth (typically the Forristall distribution is used but this can be modified to fit water depth or swell characteristics where appropriate). Then (h) we add crest, surge and tide components per sea state to obtain TWL. Finally (i) the maximum value of TWL (per directional-seasonal covariate bin) is saved for the realisation.

To obtain a single realisation of maximum TWL corresponding to a period of N years, we simply simulate the appropriate (random) number of storm events for N years, and retain the maximum value of TWL (per directional-seasonal covariate bin) over all events.

In this way, the distribution of N-year maximum TWL can therefore be estimated from multiple N-year simulations, for any combination of directional-seasonal covariate bins of interest (including the combination of all covariate bins). Typically, to estimate the distribution of N-year maximum TWL, at least 200 realisations of N-years of data are calculated so that the central characteristics (e.g. mean, median, mode) of the distribution of the N-year maximum TWL are estimated reliably. In the current work, 300 realisations of N years were evaluated. To estimate extreme quantiles (e.g. the 95%ile) of the distribution of the N-year maximum TWL precisely, a larger number of realisations would be required.

We note in passing that the computational efficiency of naive numerical simulation can often be considerably improved using e.g. numerical integration (e.g. Ross et al., 2017), importance sampling or other more thoughtful *smarter simulation*.

8. Estimation of the distribution of the *N*-year event

To estimate the distribution of the N-year maximum for quantities of interest, CEVA uses a Monte Carlo approach to simulate all storms in a return period of interest multiple times by (a) fitting the Poisson and GP model to n_B different bootstrap resamples of the original data, and (b) making n_R realisations of TWL (and its components) the full return

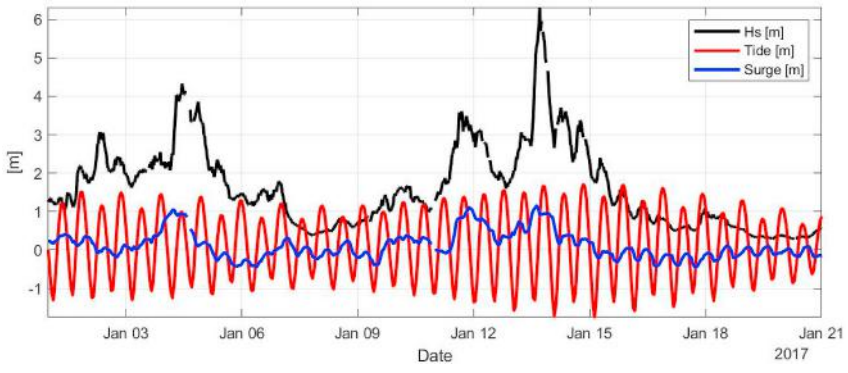

Fig. 10. Time series of H_S, surge and tide for a shallow-water location (21.0 m) showing the impact that tide can have on the variation in H_S through storms.

period of interest for each bootstrap. This produces $n_B \times n_R$ different realisations of the return period of interest, where each version consists of multiple storms each of which are simulated as described in Section 7 and from which just the largest values of H_S, individual wave height (H), individual crest height (C) and TWL are stored for every bin. This allows a probability distribution to be developed for the maximum of each of these variables for a return period of interest. The distribution of the N-year maximum for each bin can then be summarised by the quantile with non-exceedance probability $1/e$ (i.e. the 37th percentile), which corresponds to the N-year return value for that bin in the absence of parameter uncertainty. Other quantiles of the distribution can also be used, e.g. to summarise the width of the distribution of the N-year maximum.

Aleatory (natural inherent) and epistemic (data and modelling) uncertainties are captured throughout the simulation process. Natural variability of storm peaks for a given environment, of storm trajectories given storm peak, of wave heights and crests given storm trajectory and of tide are all quantified. Modelling uncertainty due to a finite original sample and choice of EV threshold is also quantified. The resulting probability distribution implicitly reflects these uncertainties. Typically, for applications to estimation of extreme wave environments based on hindcasts or measurements, the aleatory uncertainty is the major contributor to the width of the distribution of the N-year maximum.

In the example used here, only 15 realisations of 20 bootstraps of the original sample were taken; that is, 300 simulations overall have been used to illustrate the methodology. Using these simulations, the overall fit of the H_S model to the data as split by direction and season and overall are shown in Fig. 11 split by direction. A similar plot, split by season, was also inspected. This is quite a small number of realisations to estimate the whole distribution, and is reflected in the jagged nature of the modelled median and 95% UI (black) lines fitted to the observed data (red dots); as noted earlier however, 300 realisations is sufficient to estimate the central features (e.g. median) of the

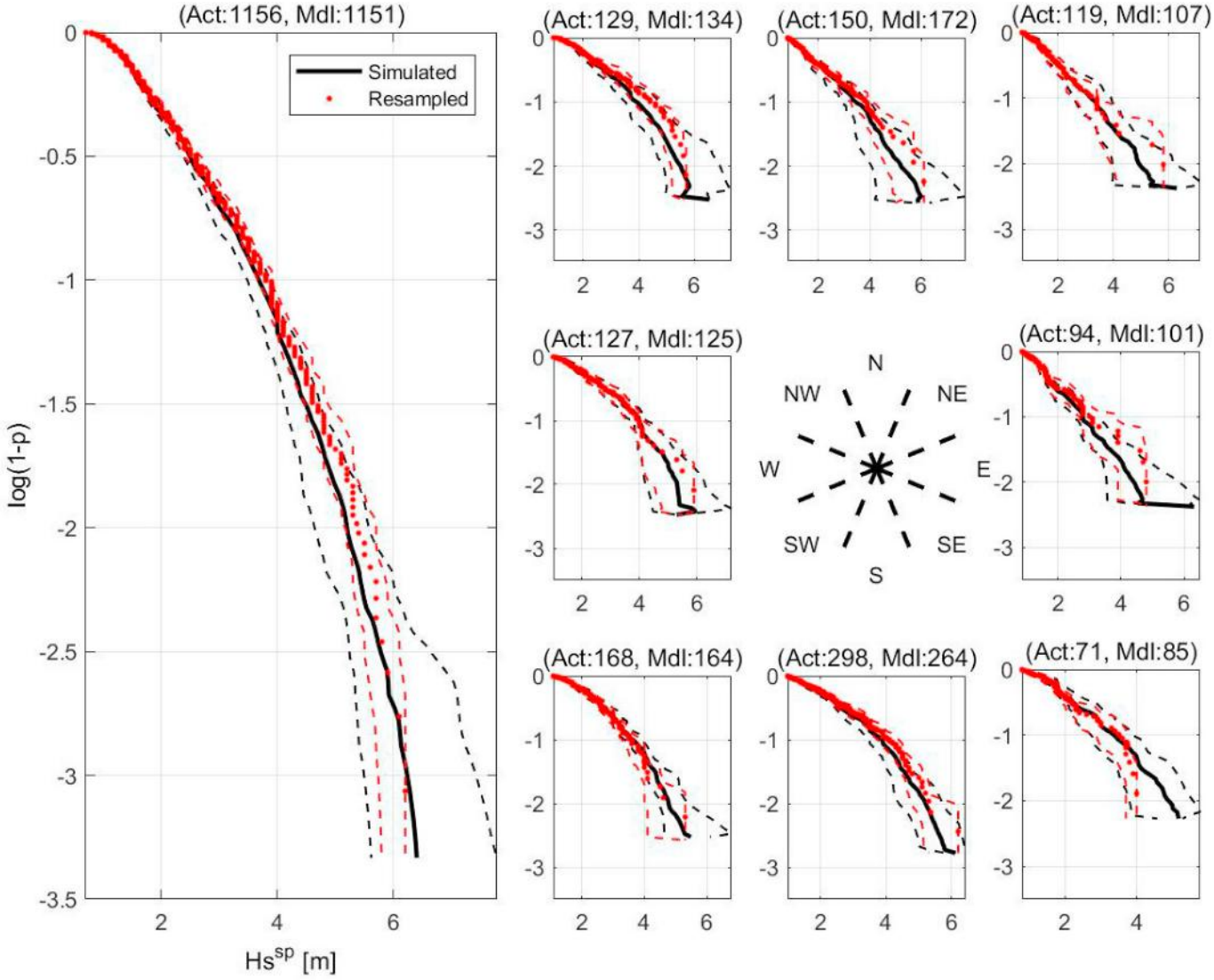

Fig. 11. Comparison between resampled underlying data (red) and simulated (black) storm peaks for the overall case (left) and for each directional sector. Solid lines represent median case, dashed lines represent the 95% uncertainty intervals. The original data is shown as red dots. Similar plots are available resolved by month. (For interpretation of the references to colour in this figure legend, the reader is referred to the Web version of this article.)

distribution. The red dashed lines represent the 95% UI range from across all bootstrap resamples. Using more realisations would make the tails smoother or, alternatively, numerical integration can also be used. The overall comparison is good with the tail corresponding to the original data being contained within the 95% UI for the tail simulated under the fitted model. Towards the top end of the data sets, the 95% UI associated with the (red) bootstrap re-sampled data narrows because the same data points are being re-sampled each time.

Similar plots are shown in Fig. 12 for all storm sea states as opposed to just the storm peaks split by direction. Plots split by month are also available. Again the overall comparison is good although the storm lengths seem to be under-estimated by the approach since the number of modelled sea states (indicated by the number to the right of Mdl above each plot) are lower than the actual (Act) number of sea states. Nevertheless, the overall comparison of the probability distributions is good.

From the 300 simulations, the distributions of the maxima are shown in Fig. 13 in which larger overall widths of the curves indicate a higher level of variability. The 37th percentile and median values are indicated by the dashed horizontal lines. The overall curves for the 37th percentile of the distribution of the N-year maxima for H_S, C and TWL are shown in Fig. 14 and Fig. 15.

Fig. 16 shows a comparison between the observed combinations of H_S and surge that were observed overall and in each directional sector overlaid by median and 95% UI shown as red lines. The equivalent modelled values are represented by the black lines. Agreement between observed (red) and simulated (black) curves is good in the body of the data, becoming more uncertain for large H_S where (a) there are fewer data and (b) there is greater spread in surge for given H_S. The differences in the relationships in each directional sector are quite clear with many sectors exhibiting an increasingly negative surge as storms become more severe, particularly from the South-East. The North-West and North on the other hand show a positive correlation between H_S and surge. These reflect the different storm tracks taken by storms which produce northerly as opposed to southerly or easterly winds at the site which will in turn affect the magnitude of the inverse

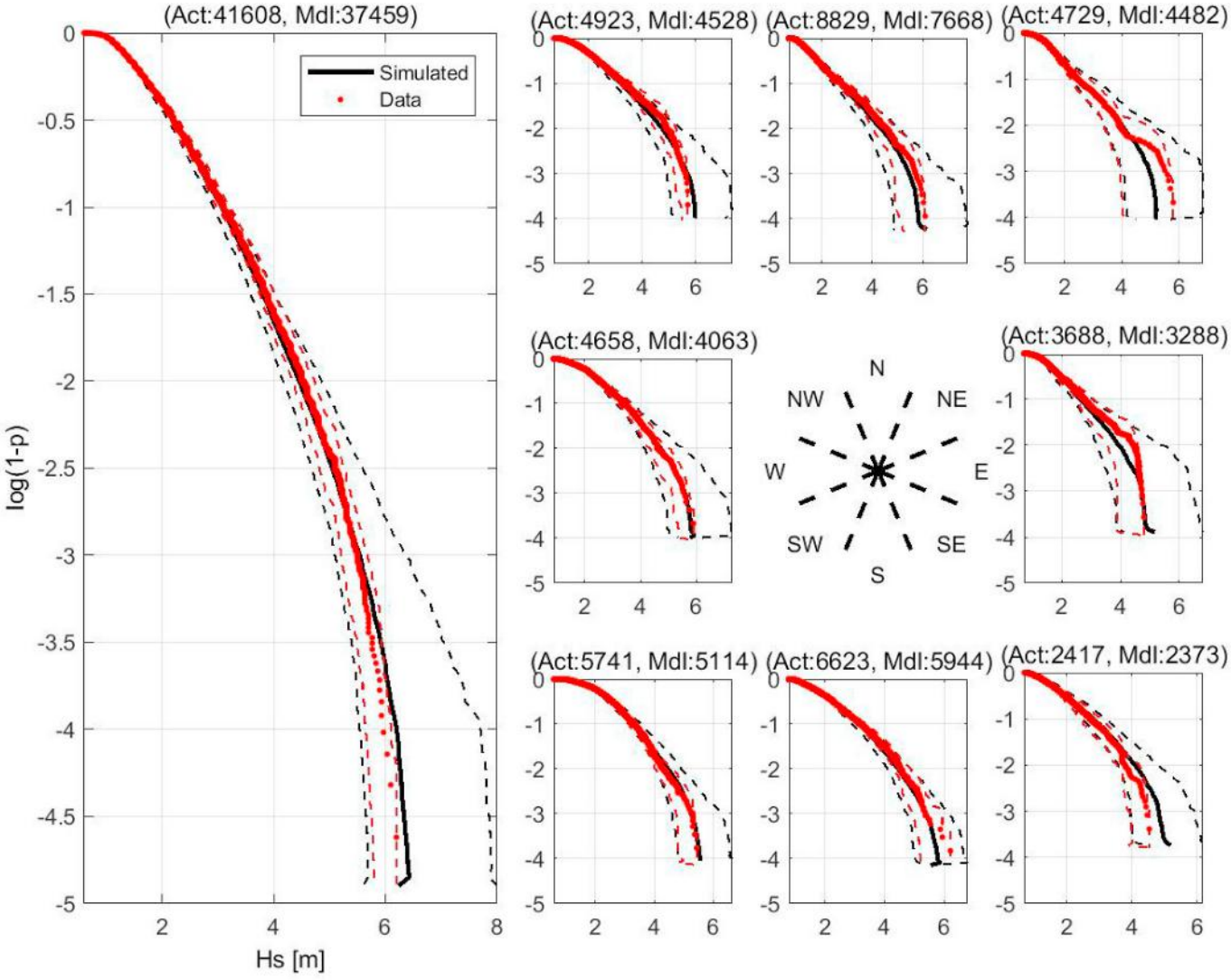

Fig. 12. Comparison between resampled underlying data (red) and simulated (black) all storm sea-states for the overall case (left) and for each directional sector. Solid lines represent median case, dashed lines represent the 95% uncertainty intervals. The original data is shown as red dots. Similar plots are available resolved by month. (For interpretation of the references to colour in this figure legend, the reader is referred to the Web version of this article.)

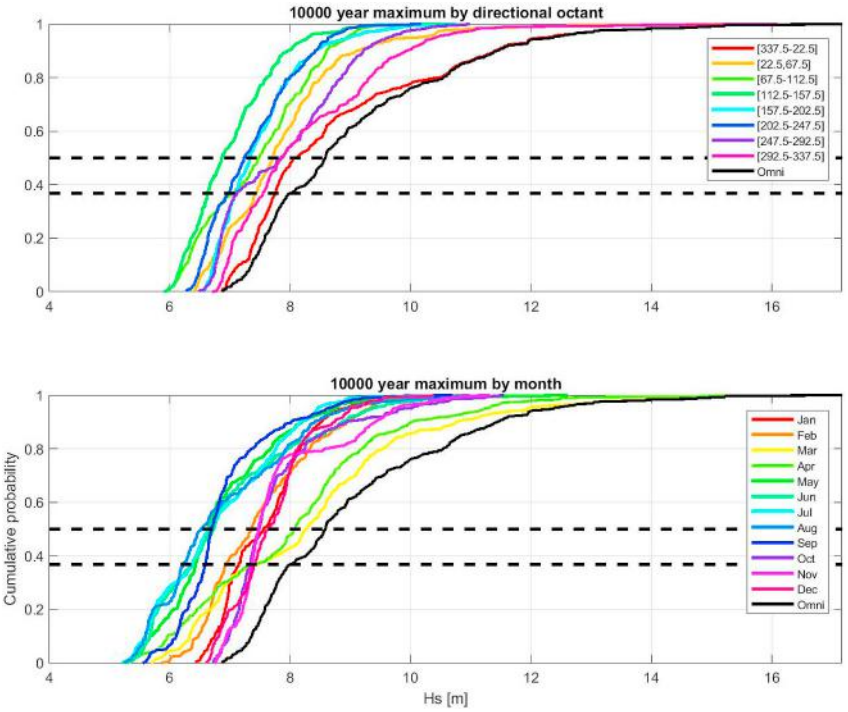

Fig. 13. Distribution of the 10,000-year maximum of H_S (a) by direction and (b) by season. In each case, the overall *omni-covariate* curve is shown in black.

barometric effect and the relative timing of the peak in surge and the H_S peak in the different storm types.

Estimates for the 37th percentile of the distribution of the *N*-year maximum for splits by direction are shown in Table 1 and Table 2 for wave crest and TWL, respectively. Equivalent tables for results split by month are shown in Table 3 and Table 4. Differences between TWL and crest values in the tables are termed *implied SWL* values and are given in Table 5 and Table 6 for values split by direction and season, respectively. We note that, for any *N*-year period, the implied SWL should be interpreted as the value of SWL that, when added to the 37th percentile of the distribution of *N*-year maximum of individual crest, provides the 37th percentile of the distribution of *N*-year maximum TWL. The term *implied SWL* is used since the largest TWL will not necessarily occur at the time of maximum individual crest height. This effect will become more significant at a location where the wave climate is not that severe and the tides are large. These tables show the varying level of contribution by directional sector as reflected in Fig. 16. Overall, the implied SWL values are larger for the North and North-West sectors than for the other sectors albeit with some variability. This could be associated with noise due to insufficient realisations in the analysis or it

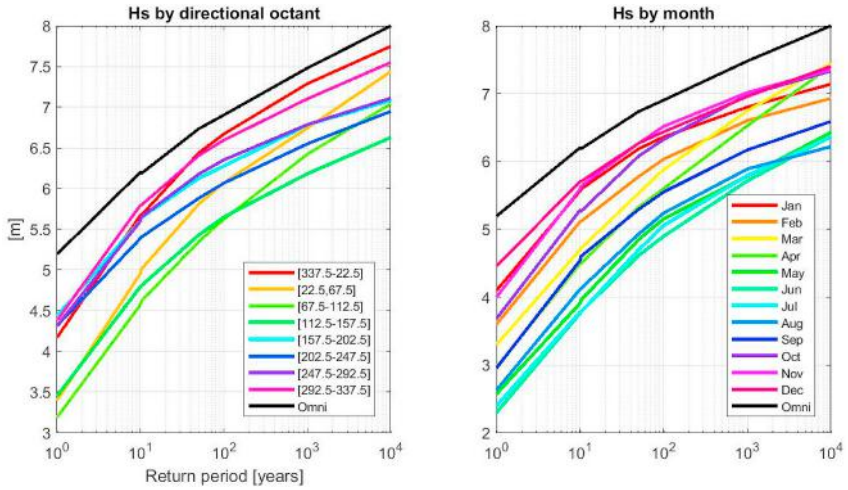

Fig. 14. 37th percentile of the distribution of *N*-year maximum H_S (a) by direction and (b) by season, by return period. The overall omni-covariate curve is shown in black.

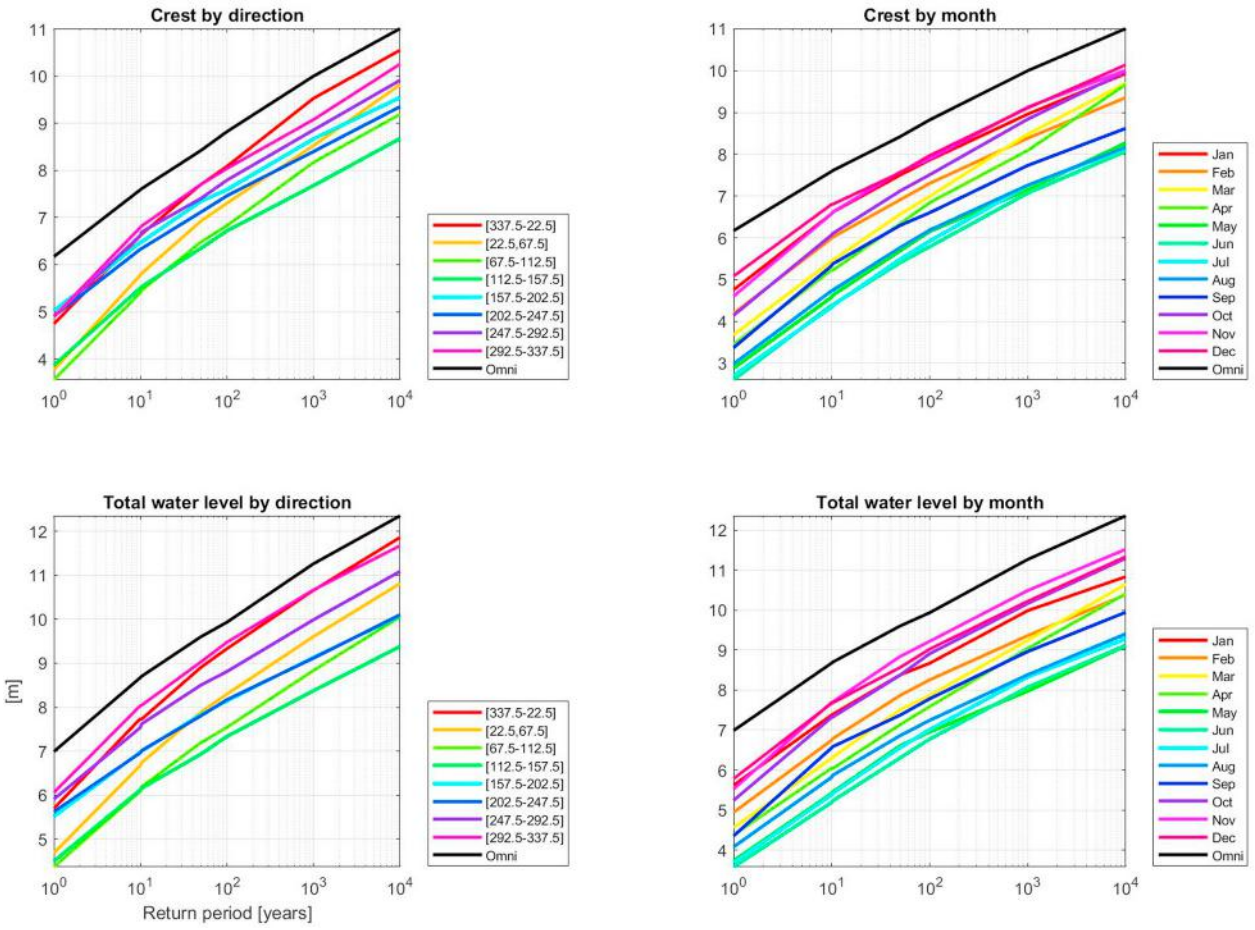

Fig. 15. 37th percentile of the distribution for *N*-year maximum (a) wave crest by direction, (b) wave crest by season, (c) total water level by direction, and (d) total water level by season, as a function of return period. The overall omni-covariate curve is shown in black.

may indicate a varying degree of association between the timing of maximum surge and maximum wave conditions across the directional-seasonal domain.

9. Discussion and conclusions

In addition to the derivation of extreme H_S and individual wave height, the covariate extreme value approach (CEVA) allows for the natural variability in waves and SWL and their joint probabilities to be modelled over long periods of time. This allows estimation of the joint distribution of *N*-year maxima of wave crest, storm surge and tide, and hence TWL. The approach includes the capability of reflecting the variability of climate with direction and season and also the correlation between the various components being studied in a non-parametric fashion which makes the approach very general.

There are some limitations to the approach, however, the main one being that sufficient storm events need to be available in the underlying data set in order to populate the many directional-seasonal bins adequately at the start of the analysis. Where data sets are shorter, or fewer events occur per year (for example, for tropical cyclones) this can be a problem, but the analysis can be carried out in with just one covariate in this case (typically direction) to increase the number of events per underlying bin. However, this still may result in poor model fits if the data set is too small. A further difficulty of the approach is that in order to get statistically stable results a large number of realisations needs to be run and this can be time-consuming even with good computing resources. Using parallel processing is a significant help in this regard, but the end-point of the development is *smarter simulation* incorporating clever sampling, numerical integration and parallel processing rather than naive Monte Carlo analysis for long return periods. A further enhancement that is under development (Ross et al., 2018) for inclusion within CEVA is the use of the approach of Heffernan and Tawn (2004) to determine the associated surge characteristics rather than using the linear regression and residuals approach described here. It is also understood that the surge and wave trajectory re-scaling approaches are relatively crude and more sophisticated statistical approaches (e.g. Tendijck et al., 2018) are being developed to describe those more systematically. Despite the limitations described here, the overall approach has been shown to produce good results in several of the major oil and gas basins and allows the complexity of the environment to be well captured within a single analysis.

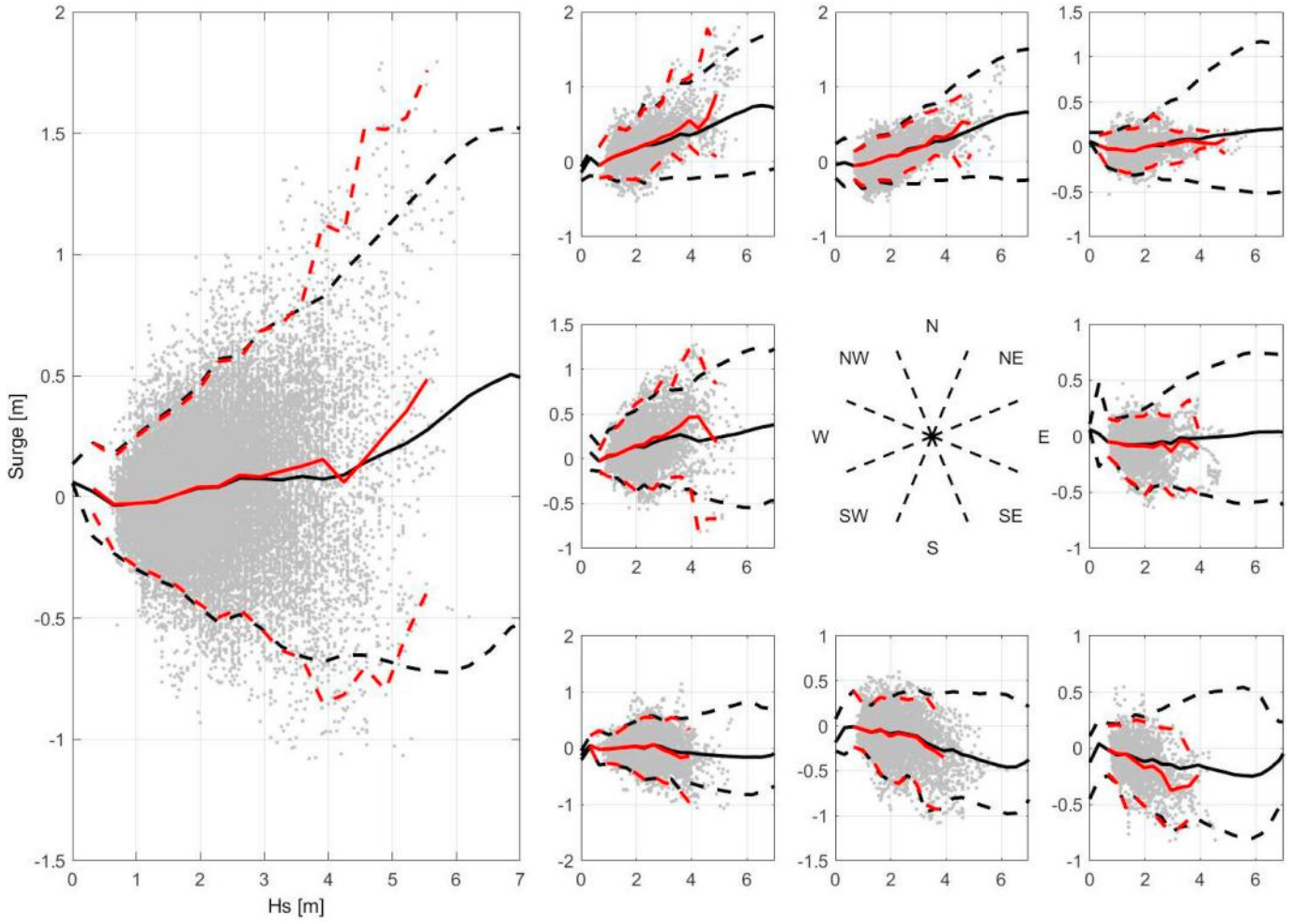

Fig. 16. Comparison of observed (red) and simulated (black) median and 95% uncertainty intervals for storm surge versus H_S. Actual historical pairs of seat state H_S and surge are given as grey dots. (For interpretation of the references to colour in this figure legend, the reader is referred to the Web version of this article.)

Table 1
Estimates for the 37th percentile of the distribution of the N-year maximum wave crest (in metres) for 8 directional octants and omnidirectionally, as a function of return period.

Crest	Return Period [years]					
	1	10	50	100	1000	10000
N	4.7	6.6	7.7	8.1	9.5	10.6
NE	3.8	5.8	6.9	7.3	8.5	9.8
E	3.6	5.4	6.5	6.8	8.2	9.2
SE	3.9	5.5	6.3	6.7	7.7	8.7
S	5.0	6.5	7.3	7.6	8.7	9.5
SW	4.9	6.3	7.1	7.5	8.4	9.4
W	4.9	6.6	7.4	7.8	8.9	9.9
NW	4.9	6.8	7.7	8.0	9.1	10.3
Omni	6.2	7.6	8.4	8.8	10.0	11.0

Table 2
Estimates for the 37th percentile of the distribution of the N-year maximum TWL (in metres) for 8 directional octants and omnidirectionally, as a function of return period.

TWL	Return Period [years]					
	1	10	50	100	1000	10000
N	5.7	7.7	8.9	9.3	10.7	11.9
NE	4.7	6.7	7.9	8.3	9.6	10.8
E	4.4	6.1	7.2	7.5	8.8	10.1
SE	4.5	6.1	6.9	7.3	8.4	9.4
S	5.5	7.0	7.8	8.1	9.1	10.1
SW	5.6	7.0	7.8	8.2	9.1	10.1
W	5.9	7.5	8.5	8.8	10.0	11.1
NW	6.1	8.0	9.0	9.5	10.7	11.7
Omni	7.0	8.7	9.6	9.9	11.3	12.4

Table 3
Estimates for the 37th percentile of the distribution of the N-year maximum wave crest (in metres) per month and all-year (over all months), as a function of return period.

Crest	Return Period [years]					
	1	10	50	100	1000	10000
Jan	4.8	6.6	7.5	7.9	9.0	9.9
Feb	4.2	6.0	6.9	7.3	8.4	9.4
Mar	3.7	5.4	6.6	7.0	8.5	9.7
Apr	3.4	5.2	6.3	6.8	8.1	9.7
May	2.9	4.6	5.7	6.2	7.2	8.3
Jun	2.6	4.4	5.4	5.8	7.1	8.1
Jul	2.7	4.3	5.5	5.9	7.2	8.1
Aug	3.0	4.7	5.8	6.2	7.3	8.2
Sep	3.4	5.3	6.3	6.6	7.7	8.6
Oct	4.1	6.1	7.1	7.5	8.8	10.0
Nov	4.6	6.6	7.6	7.9	9.1	10.0
Dec	5.1	6.8	7.6	8.0	9.1	10.1
All Year	6.2	7.6	8.4	8.8	10.0	11.0

Table 4
Estimates for the 37th percentile of the distribution of the N-year maximum TWL (in metres) per month and all-year (over all months), as a function of return period.

TWL	Return Period [years]					
	1	10	50	100	1000	10000
Jan	5.6	7.4	8.4	8.7	10.0	10.8
Feb	4.9	6.7	7.9	8.3	9.4	10.4
Mar	4.6	6.3	7.5	7.9	9.2	10.6
Apr	4.4	6.0	7.1	7.6	9.0	10.4
May	3.7	5.4	6.6	7.0	8.0	9.1
Jun	3.6	5.2	6.3	6.8	8.1	9.1
Jul	3.7	5.4	6.6	7.0	8.3	9.3
Aug	4.1	5.8	6.9	7.2	8.4	9.4
Sep	4.4	6.6	7.4	7.8	9.0	9.9
Oct	5.2	7.3	8.4	8.9	10.2	11.3
Nov	5.5	7.7	8.8	9.2	10.5	11.5
Dec	5.8	7.7	8.6	9.0	10.2	11.3
All Year	7.0	8.7	9.6	9.9	11.3	12.4

Table 5
Estimates for difference (in metres) between the 37th percentile of the distribution of the N-year maximum TWL and the 37th percentile of the distribution of the N-year maximum wave crest for 8 directional octants and omnidirectionally, as a function of return period.

Implied SWL	Return Period [years]					
	1	10	50	100	1000	10000
N	0.9	1.1	1.2	1.2	1.1	1.3
NE	0.9	0.9	1.0	1.0	1.1	1.0
E	0.8	0.7	0.7	0.7	0.7	0.9
SE	0.6	0.6	0.6	0.6	0.7	0.7
S	0.5	0.5	0.5	0.6	0.5	0.5
SW	0.7	0.6	0.7	0.7	0.7	0.8
W	1.0	0.9	1.1	1.0	1.1	1.2
NW	1.2	1.2	1.3	1.4	1.6	1.4
Omni	0.8	1.1	1.2	1.1	1.3	1.4

Table 6
Estimates for difference (in metres) between the 37th percentile of the distribution of the N-year maximum TWL and the 37th percentile of the distribution of the N-year maximum wave crest per month and all-year (over all months), as a function of return period.

Implied SWL	Return Period [years]					
	1	10	50	100	1000	10000
Jan	0.9	0.8	0.9	0.8	1.0	0.9
Feb	0.8	0.8	1.0	1.0	1.0	1.0
Mar	0.9	0.9	0.9	0.9	0.8	0.9
Apr	0.9	0.8	0.8	0.7	1.0	0.7
May	0.9	0.8	0.9	0.8	0.8	0.8
Jun	1.0	0.8	0.9	1.0	1.0	1.0
Jul	1.0	1.0	1.1	1.1	1.1	1.1
Aug	1.1	1.1	1.1	1.1	1.1	1.2
Sep	1.0	1.2	1.1	1.2	1.2	1.3
Oct	1.1	1.3	1.3	1.4	1.3	1.3
Nov	0.9	1.1	1.3	1.3	1.4	1.5
Dec	0.7	0.9	1.0	1.1	1.1	1.2
All Year	0.8	1.1	1.2	1.1	1.3	1.4

Appendix A. Supplementary data

Supplementary data to this article can be found online at https://doi.org/10.1016/j.oceaneng.2018.10.027.

References

Callaghan, D., Nielsen, P., Short, A., Ranasinghe, R., 2008. Statistical simulation of wave climate and extreme beach erosion. Coast Eng. 55 (5), 375–390.

Ewans, K.C., Jonathan, P., 2008. The effect of directionality on northern North Sea extreme wave design criteria. J. Offshore. Arct. Eng. 130, 041604:1–041604:8.

Feld, G., Randell, D., Wu, Y., Ewans, K., Jonathan, P., 2015. Estimation of storm peak and intra-storm directional-seasonal design conditions in the North Sea. J. Offshore. Arct. Eng. 137, 021102:1–021102:15.

Gouldby, B., Mendez, F., Guanche, Y., Rueda, A., Minguez, R., 2014. A methodology for deriving extreme nearshore sea conditions for structural design and flood risk analysis. Coast. Eng. 88, 15–26.

Hawkes, P.J., Gouldby, B.P., Tawn, J.A., Owen, M.W., 2002. The joint probability of waves and water levels in coastal defence design. J. Hydraul. Res. 40, 241–251.

Heffernan, J.E., Tawn, J.A., 2004. A conditional approach for multivariate extreme values. J. Roy. Stat. Soc. B 66, 497–546.

ISO19901-1, 2005. Petroleum and Natural Gas Industries. Specific Requirements for Offshore Structures. Part 1: Metocean Design and Operating Considerations, first ed. International Standards Organisation.

ISO19902, 2007. Petroleum and Natural Gas Industries. Fixed Offshore Structures, first ed. International Standards Organisation.

Leggett, I.M., Bellamy, N.F., Fox, J.P., Sheikh, R., 2007. OMAE2007-29559: a recommended approach for deriving ISO-compliant 10,000 year extreme water levels in the North Sea. In: Proc. 26th Conf. Offshore Mech. Arct. Eng.

Liu, J.C., Lence, B.J., Isaacson, M., 2010. Direct joint probability method for estimating extreme sea levels. J. Waterw. Port, Coast. Ocean Eng. 136, 66–76.

Northrop, P., Jonathan, P., 2011. Threshold modelling of spatially-dependent non-stationary extremes with application to hurricane-induced wave heights. Environmetrics 22, 799–809.

Pawlowicz, R., Beardsley, B., Lentz, S., 2002. Classical tidal harmonic analysis including error estimates in MATLAB using TTIDE. Comput. Geosci. 28, 929–937.

Pugh, D., Vassie, J., 1978. Extreme sea levels from tide and surge probability. In: Proc. 16th Coastal Engng Conf. 1. pp. 911–930.

Randell, D., Feld, G., Ewans, K., Jonathan, P., 2015. Distributions of return values for ocean wave characteristics in the South China Sea using directional-seasonal extreme value analysis. Environmetrics 26, 442–450.

Reistad, M., Breivik, O., Haakenstad, H., Aarnes, O.J., Furevik, B.R., Bidlot, J.-R., 2011. A high-resolution hindcast of wind and waves for the North sea, the Norwegian sea, and the Barents sea. J. Geophys. Res. 116, 1–18.

Ross, E., Randell, D., Ewans, K., Feld, G., Jonathan, P., 2017. Efficient estimation of return value distributions from non-stationary marginal extreme value models using Bayesian inference. Ocean Eng. 142, 315–328.

Ross, E., Sam, S., Randell, D., Feld, G., Jonathan, P., 2018. Estimating surge in extreme North Sea storms. Ocean Eng. 154, 430–444.

Serafin, K.A., Ruggiero, P., 2014. Simulating extreme total water levels using a time-dependent, extreme value approach. Journal Geophys. Res. - Oceans 119 (9), 6305–6329.

Shevchenko, G., Ivelskaya, T., 2015. Estimation of extreme sea levels for the Russian coasts of the kuril islands and the sea of okhotsk. Pure Appl. Geophys. 172, 3537–3555.

Tawn, J.A., 1992. Estimating probabilities of extreme sea levels. J. Roy. Stat. Soc. C 41, 77–93.

Tendijck, S., Ross, E., Randell, D., Jonathan, P., 2018. A model for the directional evolution of severe ocean storms. Environmetrics, e2541. https://doi.org/10.1002/env.2541.

Tromans, P.S., Vanderschuren, L., 1995. Variable Based Design Conditions in the North Sea: Application of a New Method. Offshore Technology Confernence, Houston OTC–7683.

UK Department of Energy, 1990. Metocean Parameters - Parameters Other than Waves. Supporting Document to Offshore Installations: Guidance on Design, Construction and Certification - Environmental Considerations (OTH 89 299). Her Majesty's Stationary Office, UK).

UK Health and Satefy Executive, 2009. A Monte Carlo Approach to Joint Probability of Wave, Tide and Surge in Extreme Water Level Calculations (Research Report RR740). HSE Books, UK).

UK HMSO, 1974. The Offshore Installations (Construction and Survey) Regulations (SI 174/289). Her Majesty's Stationary Office, UK).

Wahl, T., Haigh, I.D., Nicholls, R.J., Arns, A., Dangendorf, S., Hinkel, J., Slangen, A.B.A., 2017. Understanding extreme sea levels for broad-scale coastal impact and adaptation analysis. Nat. Commun. 8, 16075.

WAMDI, 1988. The WAM model: a third generation ocean wave prediction model. J. Phys. Oceanogr. 18, 1775–1810.